JOURNAL OF PROPULSION AND POWER
Vol. 25, No. 4, July–August 2009

Preliminary Investigation on Lithium Hydride as Fuel for Solid-Fueled Scramjet Engines

D. Simone* and C. Bruno†
University of Rome "La Sapienza," 00184 Rome, Italy

DOI: 10.2514/1.39136

The aim of this work is to study the combustion of a LiH grain in a supersonic airstream, as a preliminary to investigate its potential as fuel in a solid-fueled scramjet. This hydride is interesting because it reacts exothermically with many substances and contains hydrogen, suggesting its use when a much higher density (compared with that of LH_2) would be beneficial. In fact, LiH releases H_2 and Li by thermal decomposition; at the same time, the Li produced behaves as a highly energetic fuel in the presence of a high-temperature airstream. Because of the scarce data present in literature, the thermochemical properties of LiH and its decomposition were calculated, estimated, or modeled, and issues associated with its combustion in a hot supersonic stream were investigated; a simplified physical model describing its vaporization and combustion was built that was successively simulated by means of a computational fluid dynamics code. Results show that LiH is an ideal candidate for solid-fueled-scramjet applications, behaving not only as a high-energy-density bifuel system, but also as a safe and compact hydrogen carrier. An intense flame zone is predicted to be present over the decomposing surface and downstream of the grain; the flame is stable and high temperatures (on the order of 2900 K) are obtainable. Moreover, specific impulse and thrust density predicted at a flight Mach = 7 are also interesting, being 10,000 and 200–300 m/s, respectively.

I. Introduction

LITHIUM hydride is one of the most attractive elements for hydrogen storage. Li is the lightest metal, with atomic mass 6.941, almost twice lighter than carbon, and forms the simple hydride LiH. Because of its high density ($\sim$0.8 g/cm^3) and low molecular weight (7.9), LiH is the most promising compound for applications in which weight and compactness are at a premium [1–5].

LiH as fuel for space applications was investigated for the first time at the beginning of 1958 in the United States [6]. Researchers pointed out that lack of data concerning the combustion products (such as Li_2O or LiO_2) at high temperature was a limiting factor in their studies. LiH was investigated for other applications (e.g., fusion reactors); however, few citations of LiH fuel applications are available in the open literature [2,7]. The reason is probably due to its being solid at ambient temperature; however, this feature, together with its high melting point (950 K), makes LiH suitable for hybrid propulsion.

In this context, we have carried out work to analyze the LiH propulsion potential [3,5]. Using NASA's CEA2 code [8], we have simulated calculated equilibria intended to assess LiH rocket performance with polymeric binders such as HTPB, to investigate LiH as additive to common solid propellants, or as standalone fuel in SRM; although not immediately connected to the objective of this work, the results obtained have furnished fundamental information on LiH behavior in a combustion chamber; in particular, they have highlighted the significant release at equilibrium of unburned hydrogen (favoring, as an example, postcombustion in hybrid rockets), and this suggests that its best performance can be obtained when LiH decomposes, releasing Li and H_2. A second group of simulations, intended to assess LiH performance in a hot airstream [over 1000 K from 0.5 up to 5 atm of pressure, which are the conditions expected in a scramjet (SCRJ) combustion chamber], focused on the interplay among oxygen, nitrogen, and LiH and on the equilibrium composition of combustion products. Results spurred development of a simplified model of an ideal scramjet, flying a constant-dynamic-pressure trajectory. This model has explored the effect of LiH decomposition and of liquid-Li vaporization on performance (and combustion products); results have been used to determine which reactions should be considered in our solid-fueled scramjet (SFSCRJ) combustion chamber model.

Using solid fuels in airbreathing applications involves several key issues. In fact, solid fuels have been extensively investigated in conventional solid-fueled ramjet engines; however, with all supersonic combustion research being focused on liquid fuels, solid-fuel scramjet studies are scarce or nonexistent in the open literature. The first experimental studies of a SFSCRJ were made by Witt and Angus (1989 and 1991, cited in [9]); results were used later by Angus et al. (1993, cited in [9]) to perform new experiments on a specific configuration. Following this work, an experimental investigation was performed by Ben-Yakar et al. [10]; they demonstrated, for the first time, the feasibility of self-ignition of a polymethyl methacrylate (PMMA) solid-fuel grain as well as sustained combustion under supersonic airflow conditions without external aids. Successively, Cohen-Zur and Natan [11] performed a experimental parametric investigation of the same geometrical configuration, obtaining self-ignition and flameholding characteristics consistent with [10].

Computationally, attempts to investigate the flame evolution inside the combustion chamber were made by Jarymowycz et al. [12], who conducted a comparative numerical study of combustion of hydroxyl-terminated polybutadiene (HTPB) in a supersonic flow; the flight condition at Mach 7.3 corresponded to a combustor inlet static temperature of 1400 K, with a Mach number of 2 and static pressure of 1 atm.

Solid-fuel/air mixing in a supersonic stream was addressed by Ben-Arosh et al. [13]. They investigated supersonic combustion in an axisymmetric dump combustor. The parametric investigation in the nonreacting case showed the effect of gaseous-fuel wall-injection velocity (from 0.5 up to 4 m/s), revealing that fuel/air mixing in a SFSCRJ does not limit combustion more than it does in a conventional solid-fueled ramjet. Finally, Ben-Arosh et al. developed a two-dimensional, axisymmetric, turbulent (k-ε), two-reaction, six-species reactive flow model to investigate the same configuration [9]. Results indicated high sensitivity to the design parameters, showing that an inappropriate configuration might cause flame extinction or choking.

Received 16 June 2008; revision received 12 March 2009; accepted for publication 26 March 2009.

*Ph.D., Department of Mechanics and Aeronautics, Via Eudossiana 18.
†Professor, Department of Mechanics and Aeronautics, Via Eudossiana 18. Associate Fellow AIAA.

Based on past work, LiH seems capable of overcoming at least some of the problems found with scramjet propulsion systems. That is the reason for the subsequent preliminary thermochemical analysis.

II. Thermochemical Analysis of LiH

LiH is a hydrogen-rich compound with potential application as fuel, due to its high density ($\sim$0.8 g/cm^3) and low molecular weight (MW = 7.9); some of its properties are in Table 1 [14,15].

Produced by reacting Li and H_2 at about 570 K and 1 bar, LiH is a ionic solid containing Li^+ and hydrogen H^- (14.3% in mass); it behaves as a strongly reducing agent. LiH reacts very fast with many oxidizers, halogenated hydrocarbons, and acids; its combustion products contain light molecules [1–5].

LiH reacts slowly at STP with air oxygen; at 470 K it starts to burn spontaneously on contact with air; finely dispersed particles form explosive mixtures, especially in the presence of moisture [Brinza et al. [16] have measured flame propagation rates of $\mathcal{O}(10)$ m/s]. Conversely, liquid LiH presents a high energy density (49 MJ/kg), comparable, for instance, with that of aviation kerosene (43.2 MJ/kg and the same density of LiH) [17]. The most interesting feature of LiH, however, is its ability to decompose endothermically, releasing gaseous hydrogen.

LiH liquefies at 950 K; whereas the other alkaline hydrides decompose at the melting point, liquid LiH remains stable in a narrow range of temperatures (950 K < T < 1100 K). When temperature is increased from the melting up to the boiling point, the amount of hydrogen released by thermal decomposition increases, producing a mixture of Li and LiH. The Li/LiH system is of great interest in controlled thermonuclear research and as a potential cooling system in nuclear power plants, due to its high thermal capacity at and near the melting point; however, due to the risks associated with the release of significant amounts of gaseous hydrogen, the idea of using it as cooling system was abandoned (Li remains the material of choice in the "blanket" surrounding the fusion reactor and produces tritium when crossed by fusion-produced neutrons). Although papers about the Li/LiH system thermal properties are available [18–21], data on LiH decomposition are rare or nonexistent. It is known that hydrogen also diffuses from LiH at STP conditions [22]; at the ignition point (470 K in dry air; that is, 20 K over the melting point of Li), the amount of hydrogen leaving a LiH particle is so significant that the liquid Li formed on the LiH surface can ignite, heating the hydrogen and promoting its combustion near the surface. Increasing the LiH surface exposed to air increases the amount of hydrogen (and liquid Li) delivered, and the reaction may become explosive. LiH decomposition can be considered complete right below its boiling point (1100 K at 1 atm).

Rate constants for hydrogen/Li kinetics have been computed by Mayer and Schieler [23] and Mayer et al. [24] in the temperature range 900–1200 K. Another important contribution to the understanding of issues associated with the thermal decomposition is by Jerry and Modisette [25,26], who investigated LiH as a high-temperature internal coolant for the nose of hypersonic missiles. As stated in these works, LiH exposed to a heat flux corresponding to Mach 2 flow at 2000 K can absorb up to 7 kJ/g of decomposed LiH.

Decomposition of LiH follows the equilibrium:

$$2\mathrm{LiH} \rightleftarrows 2\mathrm{Li} + \mathrm{H_2}$$

Table 1 LiH properties

Property	At melting point (950 K) [a]	At boiling point [a] (1100 K)
Density, kg/m^3	800	550
Latent heat of fusion, J/kg	2×10^6	——
Heat capacity, J/kg (K)	7900	6900
Thermal conductivity, W/(m) (K)	7.1	3.5
Thermal diffusivity, m^2/s	1.63×10^{-6}	1.01×10^{-6}

[a]At 1 atm.

Increasing temperature increases the rates of both forward and backward reactions. However, the increase in the forward reaction is much greater than in the reverse reaction, so that the overall effect of increasing temperature is to shift the equilibrium forward. In a closed vessel, the forward reaction is constrained by the increasing vapor pressure of the gaseous hydrogen produced, and equilibrium is quickly reached; if hydrogen is vented or burned, decomposition will continue indefinitely. Steady decomposition brings about an increase in the concentration of Li atoms on the surface, with an accompanying acceleration of the reverse reaction (proportional to the square of the concentrations of Li atoms on the surface), therefore lowering the equilibrium hydrogen pressure. The overall effect is an increase in the equilibrium temperature, enhancing the cooling ability of LiH.

However, in the case of a scramjet combustor, the situation is slightly different; in fact, at high ambient temperature and in high-speed flow, liquid-Li vaporization and/or dragging by the turbulent flow may increase the forward reaction rate, enabling the decomposition to proceed as fast as the thermal fluxes allow [5].

Note that recent studies of the use of metal hydrides as hydrogen storage systems for onboard applications have focused on the possibility of decreasing their decomposition temperature by reacting them with light elements or other hydrides. If confirmed, this feature will extend to low temperatures the operational range of LiH as fuel (i.e., low with respect to those considered here), enhancing its performance in the scramjet combustion chamber.

Previous results for LiH/air combustion and these considerations show that lithium [3,5], together with the hydrogen released by thermal decomposition, plays a key role in LiH performance. In fact, increasing the temperature over its autoignition point, LiH burns as an effect of liquid-Li oxidation. Locally increasing the temperature promotes LiH decomposition.

Thus, to understand what actually can happen in a combustion chamber, Li properties were investigated. A good review of lithium's properties is by Cowles and Pasternac and Ballif et al. (cited in [27]).

At room temperature, Li reacts with air and water. In particular, compact metal reacts much more slowly than finely divided Li particles (hydrogen formed does not ignite). Conversely, by adding very small amounts of Li powder to water in a test tube, both Li and hydrogen ignite and burn; increasing the amount of powder added, the reaction became more vigorous and the fine metal dust is expelled from the tube and ignites. Finally, adding a large amount of Li to a pool containing water, the reaction becomes violent and the hydrogen formed ignites together with lithium, leading to an intense flame near the surface; the Li expelled reacts with air and strongly alkaline LiOH is formed in the solution [27].

At high temperatures, molten Li reacts with all known molecular gases, but it can be safely handled up to 473 K in paraffin. Liquid Li is considered inert in He under most conditions. Small amounts of moisture catalyze Li/gas reactions. In particular, liquid Li will not react with oxygen or carbon dioxide at its melting point in the absence of moisture, but 10 to 15 ppm moisture is enough to allow Li to react violently with air, nitrogen, oxygen, and carbon dioxide at room temperature.

In a stream of dry nitrogen, the reaction between liquid Li and nitrogen is 10 to 15 times more rapid than in air. It was noted that oxygen and hydrogen inhibit the interaction of Li and nitrogen. In particular [27], oxygen in nitrogen at a percentage greater than 14% in volume may completely prevent reaction between Li and N_2 at lower temperatures; with less O_2, this reaction proceeds, albeit slowly.

Fires involving liquid Li are more intense than those of sodium. At 1 bar and heated to 450 K, quiescent liquid Li ignites and burns with a maximum flame temperature 1100 K measured near the surface; at relative humidity of 40 to 55% and air speed of 0 to 10 m/s, the maximum temperatures measured are greater than 1400 K.

Li was extensively investigated as coolant and tritium-breeding material for controlled thermonuclear reactors because of its low melting point, high boiling point, low vapor pressure, low density, high heat capacity, high thermal conductivity, and low viscosity (Table 2) [28–30].

Table 2 Li properties

Property	At melting point [a] (453.7 K)	At boiling point [a] (1608 K)
Density, kg/m^3	516	401
Electrical resistivity, ($\mu\Omega$) (cm)	25	57.6
Enthalpy, J/kg	1.14×10^6	5.95×10^6
Latent heat of fusion, J/kg	4.55×10^5	——
Heat capacity, J/(kg) (K)	4169	4169
Surface tension, N/m	0.396	0.24
Thermal conductivity, W/(m) (K)	44	64.7
Vapor pressure, N/m^2	1.77×10^{-8}	1.013×10^5
Viscosity, (N) (s)/m^2	0.64×10^{-3}	0.14×10^{-3}
Prandtl number	6.12×10^{-2}	8.65×10^{-3}
Thermal diffusivity, m^2/s	2.03×10^{-5}	3.86×10^{-5}

[a]At 1 atm.

Experimental and theoretical studies were performed to understand liquid-Li behavior in terms of adiabatic flame temperature, pressure rise in closed vessels, reaction rates in the presence of dry and moist air, and reactivity with vessel materials' end-reaction product toxicity [31,32]. Software was developed to accurately model liquid-Li combustion; in particular, the LITFIRE and the MELCOR codes, well documented in the open literature, present an intriguing approach to Li/air reactions [33–39]. Unfortunately, these works are limited to temperatures from 500 to 1100 K; as of today, data on reaction rates of Li with air at high temperature and chemical properties of its compounds are still scarce or nonexistent. Therefore, in [5], using the same approach of researchers at Massachusetts Institute of Technology [27,31,33,34], we have extended the lithium/air combustion analysis at temperatures higher than 1200 K. Results have highlighted that in this range of temperature, the energy release contributed by the Li/N_2 reaction is negligible; the only effect that we obtain injecting Li into a hot stream of nitrogen is to lower the mixture temperature. We have therefore investigated the combustion properties of Li released from LiH decomposition assuming only oxygen as oxidizer.

To highlight the importance of Li combustion, we have compared (using the NASA CEA2 code) the combustion of Li and of hydrogen in oxygen, assuming that both are injected at an initial temperature ranging from 1800 to 2600 K, oxygen at 1400 K, and at pressure from 0.5 atm up to 5 atm (that is, the conditions expected in a scramjet combustor).

As shown in Figs. 1 and 2, the combustion temperature of Li is slightly higher and with a broader peak than that of hydrogen at the same initial conditions.

The light and extremely reactive Li atoms freed from the LiH surface burn with oxygen, producing a mixture of oxide, peroxide, and super oxide,

$$Li + O_2 \rightarrow Li_2O + Li_2O_2 + LiO$$

that has interesting similarities with the mixture produced (at chemical equilibrium) by burning hydrogen and oxygen:

$$H_2 + O_2 \rightarrow H_2O + H_2O_2 + HO_2 + OH$$

where each of the hydrogen oxides has its counterpart in the Li oxide mixture.

Note that the CEA2 database does not currently contain the polynomial coefficients relative to Li superoxide. Although it is a significant limitation in assessing Li/O_2 chemical kinetics (as shown later), that is not significant at equilibrium: in fact, peroxide and superoxide concentrations are very small with respect to those of oxides.

From [5], the main products of LiH/O_2 and Li/O_2 reactions are, respectively, LiOH and Li_2O. However, LiOH(s) decomposes at its melting point (1200 K), which is a lower temperature than those considered, whereas Li_2O decomposes at the boiling point, yielding oxygen, liquid Li, and a little LiO.

Few data are available about Li/O_2 reactions at *high* temperature and about *gaseous* Li_2O properties; most of them are related to research on termolecular reactions of alkali metals atoms with O_2 and OH [40,41]. In particular, Plane and Rajasekhar [41], investigating the hydrogen concentration in the afterburning region of a flame, has shown that the termolecular reaction

$$Li + O_2 + N_2 \rightarrow LiO_2 + N_2 \quad (1)$$

plays an important role in Li/O_2 combustion. In fact, experimentally demonstrating reaction (1), they obtained the absolute rate constant fit over the temperature range 276–1100 K; then they extrapolated rate coefficients to flame temperatures (1500–2500 K) by means of a fit to the Troe formalism [42].

The termolecular reaction (1) involves the association of neutral fragments to form LiO_2, known to exist as an ion pair $Li^+O_2^-$; however, despite the strength of the Li/O bond, this pair is highly unstable, the reason being precisely its ionic nature. In fact, the covalent bond between the two O atoms of the peroxide ion is relatively weak; a positive ion close to the peroxide ion will attract peroxide electrons. This effect may form a simple oxide ion if the covalent bond breaks off, and it works best if the positive ion is small and has a high charge density. Even though it has only one charge, the Li ion, at the top of group I in the periodic system, is so small and therefore possesses such a high charge density that any peroxide ion near it breaks up, yielding an oxide and oxygen. The highly reactive LiO, in turn, reacts in a Li-rich environment, forming Li_2O:

$$Li + LiO \rightarrow Li_2O$$

All these association/dissociation reactions involving light alkali metal atoms have characteristic times of the same order of magnitude; at high temperature ($1500\ K < T < 2500\ K$; that is the same range expected in scramjet combustors), they can be faster than hydrogen/oxygen reactions [41]. This circumstance, suggested by similarity between the equilibrium composition of Li/O_2 and H_2/O_2 combustion products, is also confirmed thermodynamically; in fact, the reaction enthalpy and the Gibbs free energy calculated using the CEA2 polynomial coefficients in the range 800–3600 K show that the Li/LiO reaction is more exothermic than H_2/O_2 reaction. Hence, one would assume that in establishing equilibrium, the former would be preferred over the latter. Furthermore, the ΔG° is of the same order for both reactions, with the H_2/O_2 reaction slightly favored with respect to Li/LiO reaction at higher temperatures (when Li_2O

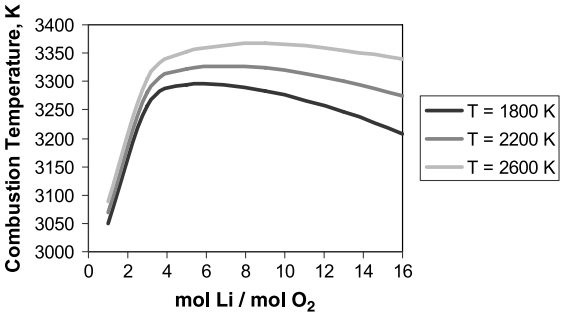

Fig. 1 Li/O_2 equilibrium combustion temperature (1 atm).

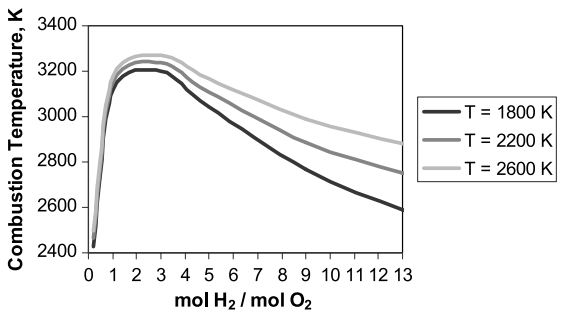

Fig. 2 H_2/O_2 equilibrium combustion temperature (1 atm).

decomposes), indicating that both forward reactions are carried to completion with a comparable rate.

Thus, it appears reasonable and expedient (e.g., lacking other rate data) to assume reaction (1) as the reaction rate for the lithium/oxygen combustion [41].

Note that Li also reacts with radicals produced by the H_2/O_2 combustion (OH, HO_2); despite the very high reaction enthalpies, these reactions can be neglected, either because the radical concentration is small or because by increasing the temperature, the reaction becomes gradually more constrained by thermodynamics (as in the case of Li/OH reaction: in fact, its ΔG° becomes greater than 0, starting from 1500 K) [5].

III. Physical Model

All of the issues concerning LiH thermal decomposition and reactions with air must be investigated within the scramjet flowfield. Here, due to the compression operated by the inlet oblique shock system assumed, the supersonic airflow in the combustor possesses high temperature and high dynamic pressure. Entering into the combustion chamber, air flows over the solid grain and forms a turbulent compressible boundary layer while the grain surface regresses. The mass evolved from the fuel surface is injected into this boundary layer and increases its thickness. Thus, for combustion to occur inside the boundary layer and/or into the core flow, the fuel must react with the hot airstream in a few milliseconds to produce the heat fluxes necessary to gasify the solid LiH grain. For these reasons, species diffusion into the hot stream and their reaction rate with air are critical issues that, in general, make gaseous hydrogen preferable as fuel for scramjet application. The behavior of LiH (which can decompose very fast, releasing gaseous hydrogen and light, highly reactive lithium) offers an ideal solution to both hydrogen storage and high-energy-density problems. Based on thermochemical-property information and on the flow conditions into the combustion chamber summarized in Sec. II, we next list and justify each model assumption by means of an order-of-magnitude analysis [5]. Accordingly, the grain combustion will be described by the following steps:

1) The LiH grain surface liquefies due to the thermal fluxes produced by combustion in the gas phase; in this phase change we assume the solid/liquid interface (or wall) to be always at the LiH liquefaction temperature ($T_{liq} = 950$ K at 1 atm).

2) Because of the high thermal diffusivity of liquid LiH, the LiH droplets formed at the wall and heated by the thermal flux reach the LiH decomposition temperature ($T_{dec} = 1100$ K). LiH decomposes fast (i.e., compared with the combustor convective time and before reacting with oxygen), its decomposition time is on the order of 10^{-6} s [23,24]; in fact, the LiH reaction rate with oxygen is lower than its decomposition rate (at least by 3 orders of magnitude), and the oxygen concentration near the surface is too small to allow significant oxidation [12,42]. As stated previously, LiH does not react with air nitrogen in this range of temperatures.

3) Following decomposition, gaseous hydrogen leaves the droplet surface bubbling vigorously and contributing to its fragmentation into smaller liquid-Li droplets [25,26]. Hydrogen diffuses through the boundary layer, mixes with air oxygen driven by the highly turbulent stream, burns, and releases heat. Some Li particles may be trapped into the hydrogen bubbles leaving the surface, burn with oxygen, and increase the heat released by hydrogen combustion.

4) Liquid-Li droplets are sheared and dragged away from the surface and into the turbulent boundary layer.

5) The light Li droplets are thus mixed with air and hydrogen combustion products present in the boundary layer. In the hot core flow they vaporize, yielding highly reactive gaseous Li. Carried by the turbulent stream, Li burns with air oxygen and with radicals produced by hydrogen combustion. When allowed by the local oxygen concentration, Li combustion occurs in proximity of the droplet surface, enhancing liquid-Li vaporization.

6) When combustion is well developed, the water vapor concentration is so high that it can react with the liquid LiH near the surface; however, the LiOH so produced at these temperatures decomposes, yielding liquid Li and OH.

To conservatively assess the effect of heat fluxes on the surface, LiH liquefaction rate can be roughly estimated by neglecting the effect of combustion heat transfer and accounting only for the convective heat fluxes and shear stresses due to the airstream entering the chamber, also assuming that the heat absorbed locally by the interface is the sum of the latent heat of liquefaction (see Table 3) and the heat required to increase the liquid-LiH temperature from 950 to 1100 K ($\Delta H = 875$ kJ/kg).

Because the thermal diffusivity of liquid Li is $D^{\text{th}} \approx 10^{-6}$ m^2/s, the characteristic heating time of a 1-μm-deep liquid layer is about 10^{-6} s; thus, we can assume the liquefaction and heating processes to happen in a single step, with a total local heat required of about 3400 kJ/kg. For instance, for a thermal flux $q_w \approx 1$ MW/m^2, the local mass flux is $m_f \approx 3 \times 10^{-4}$ g/s (the liquid-LiH density $\rho_l = 5 \times 10^{-4}$ g/mm^3), corresponding to a local regression rate of about 0.6 mm/s. As the convective time is on the order of 10^{-3} s, the thickness of the liquid layer formed during 1 ms on the surface is $h_l \approx 0.6$ μm. Note that the surface regression rate is slightly lower than typical regression rates of solid fuels. However, in this conservative analysis, the heat flux contribution due to gas-phase reactions was neglected; in reality, this contribution will strongly enhance the combustion performance by increasing the regression rate and thus the amount of gaseous fuel produced. An example of the thermal power available if all the fuel mass flow rate calculated ($m_f = 3 \times 10^{-4}$ g/s) reacted in the gas phase is given in Table 4, in which the thermal power from Li in m_f (assumed to react completely following one among the four reactions) is compared with that of the reaction between the hydrogen contained in m_f and air oxygen.

IV. Grain Regression Model

A solid-fueled scramjet has many similarities with hybrid rockets: the oxidizer diffuses into the boundary layer and reacts with the gaseous fuel pyrolyzed and released by the solid grain surface. Accounting for specific differences, it is thus reasonable to assume one among the well known models present in the open literature to predict surface regression.

The most plausible (and used) model of hybrid combustion was developed by Marxman and Gilbert (1963, cited in [43,44]). In this model, the grain regression rate is governed by the local thermal flux at the surface:

Table 3 Solid fuels for SCRJ applications: thermal properties comparison

Fuel	Average molecular formula	Mass density, kg/m^3	Molar mass, kg/k mol	ΔH_f° kJ/mol	Melting point, K	Thermal conductivity, W/(m · K)	Heat of gasification, kJ/kg
Plexiglass (PMMA)	$(C_5H_8O_2)_n$	1180	100	−430.5	527.6	0.17–0.19	1300–2700
Polyethylene	$(C_2H_4)_n$	910–965	28	−53.8	400	0.40–0.46	3000–5600
Polystyrene	$(C_8H_8)_n$	1050	104	+18.4	510	0.1–0.13	2700
HTPB	$(C_{10}H_{15,538}O_{0,073})_n$	930	138	−51.8	N/A	0.217	1800
LiH	LiH	800	7.9	−90.63	950	7.1	2625 [a]

[a]Latent heat of liquefaction.

Table 4 Thermal powers corresponding to m_f

Reactants	Products	$\Delta H_{\text{reaction}}$, KJ/mol	Thermal power, W/mm^2
Li + O2	Li2O	242	10.9
Li + O2H	Li2O + H	435	19.6
Li + O2H	LiOH + O2	600	27
Li + OH	LiOH	633	28.5
H2 + O2	H2O	253	5.7

$$\rho_g v_g = (\rho v)_w = \frac{\dot{q}_w}{H_v} \tag{2}$$

where ρ_g is the density, v_g the velocity of the gaseous fuel leaving the surface, $\dot{q}_w$ (J/m^2 s) is the heat flux at the wall, and H_v (J/kg) is, in general, the total heat required to gasify the solid fuel. In the case of a LiH grain, the surface temperature is that of the phase change (LiH solid to liquid; 950 K), and H_v accounts for the heat necessary to vaporize and decompose LiH ($H_v \sim 11$ MJ/kg).

The equation describing the regression rate $\dot{r}$ is

$$\rho_s \dot{r} = \rho_g v_g = (\rho v)_w = \frac{\dot{q}_w}{H_v} \tag{3}$$

Thus, the key point of the model is to estimate the heat flux at the surface; neglecting the conduction heat exchange inside the grain, the total thermal flux is the sum of radiative and convective heat fluxes. The latter, in turn, may be affected by the injection of gaseous fuel (at 950 K) from the surface.

To assess the impact of fuel injection from the surface (blowing) on the convective heat flux, we must account for its influence on the local boundary-layer velocity profile. The first theoretical analysis of blowing was made in 1942 by Schlichting [45]; successively, experimental as well as theoretical investigation have been performed by Rotta (as described by Schlichting [45], page 645), and the injection of a gas through a porous wall into a compressible flow, up to Mach 3.6, was investigated by Squire (as described by Schlichting [45], page 647); calculations showed that Rotta's assumptions were still valid, leading to satisfactory results. Using Rotta's empirical formulation, it is possible to show that [5] at high temperature (1450 K) and flow velocity (1400 m/s condition expected in the case under examination) and for regression rates on the order of 1 mm/s or less, the impact of blowing on wall velocity profiles and heat fluxes is negligible. This assumption, however, does not account for the cooling effect due to the gas injection temperature; furthermore, Rotta's model is strictly valid for a flat plate and may not be appropriate in a flameholder recirculation zone or in regions with shock/boundary-layer interactions. In these regions, the blowing effect will be investigated, analyzing simulation results.

V. Numerical Simulations

In simulating combustion in a LiH-fueled SFSCRJ, we have investigated geometrical configurations and flight conditions similar to those in [12]; in particular, we have selected the following combustor inlet conditions: inlet Mach number is 2, static temperature is 1500 K, static pressure is 1 atm, total pressure is 7.8 atm, and flow velocity is 1490 m/s.

The geometries considered in this analysis (hereinafter referred to as cylindrical and dump combustors, respectively) are shown in Fig. 3.

Similar to [12,13], the LiH grain is located along the upper surface of the 2-D half-section, with an inlet height of 5 cm; the LiH grain, 60 cm long, starts 5 cm from the inlet entrance and ends 40 cm from the combustor exit. The last 40 cm are assumed to be adiabatic. The dump ratio D_r is defined as

$$D_r = \frac{R_c}{R_i}$$

where R_c is the combustor internal radius and R_i is the inlet internal radius. A control line (half-radius line) located at $R_c/2$ will be used to plot pressure and temperature along the combustor. The dump height is $R_c - R_i$.

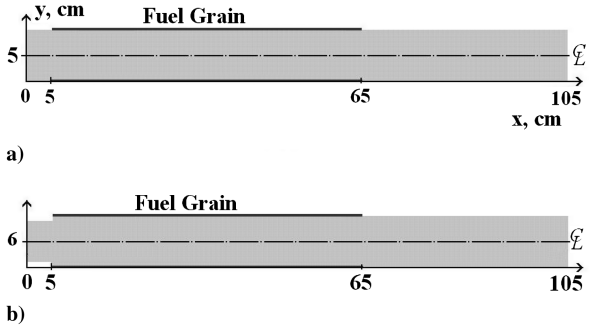

Fig. 3 Combustors: a) cylindrical ($D_r = 1$) and b) dump1 ($D_r = 1.2$).

The dump1 combustor differs from the cylindrical one by the presence of a sudden expansion with a dump height of 1 cm.

The third dump configuration simulated (dump05) differs from dump1 only in the dump height (0.5 cm).

Simulations were carried out using Favre-averaged Navier–Stokes and an axisymmetric domain with FLUENT 6.2.16 [46]. The numerical technique is a finite volume approach with quadrilateral control volumes and structured Cartesian mesh. In particular, the cylinder (Fig. 3a) has a grid composed of 155,000 cells: in the longitudinal direction, the grid spacing is uniform (0.5 mm) over the grain. The mesh increases exponentially downstream of the grain, with the largest spacing being 2 mm in length. In the vertical direction, the grid spacing changes exponentially, with the smallest spacing (near the surface) being 50 μm.

The dump1 combustor (Fig. 3b) has 216,900 cells; in the longitudinal direction and over the grain the grid spacing is a uniform 0.25 mm. The mesh increases exponentially (exponential ratio of 0.1) downstream of the grain; the largest spacing is 2 mm long. In the vertical direction, the spacing increases with an exponential ratio of 0.11. The dump05 grid consists of 169,200 cells. Over the grain, the constant grid spacing is again 0.25 mm. Downstream of the grain, the mesh increases exponentially (exponential ratio 0.11), with the largest spacing measuring 2 mm. In the vertical direction, the grid has an exponential progression ratio.

Even though blowing may lead to intrinsic instabilities [47], a steady-state solution was sought using a coupled, implicit, second-order upwind scheme. Turbulence was modeled using a standard k-ε model [9–13,46,47]. The boundary conditions at the interface between regressing grain and gas required detailed considerations and are presented in the following section.

To simulate gas-phase combustion, a six-species simplified mechanism was adopted involving the following reactions:

LiH decomposition [23,42]:

$$\text{LiH} \rightarrow \text{Li} + \tfrac{1}{2}\text{H}_2$$

One-step reaction for hydrogen combustion [42,46]:

$$\text{H}_2 + \tfrac{1}{2}\text{O}_2 \rightarrow \text{H}_2\text{O}$$

One-step reaction for Li oxidation [40–42]:

$$2\text{Li} + 1/2\text{O}_2 \rightarrow \text{Li}_2\text{O}$$

This mechanism does not account for backward reactions, because their characteristic times are larger than their convective times. The coupling between chemical kinetics and turbulence is modeled using the eddy dissipation concept model [5,46].

Thermodynamic data have been calculated using the CEA2 database; in particular, C_p of individual species was calculated by fitting CEA2 data with third-order polynomials from 300 to 6000 K, successively implemented in the code.

The molecular viscosities μ_i in the same temperature range were calculated from kinetic theory using the following equation:

$$\mu_i = \frac{2}{3}\frac{1}{\sigma_i}\sqrt{\frac{m_i kT}{\pi}}$$

where $k = 1.38 \times 10^{-23}$ J/K is Boltzmann's constant, m is the molecular mass, and $\sigma = \pi d^2$, where d is the molecular diameter. Viscosities were interpolated by third-order polynomials.

To model blowing, mass, momentum, and energy sources were imposed at the first cell above the wall (assumed impermeable and adiabatic) (Fig. 4).

These source terms S_ϕ appear in the generic transport Eq. (4):

$$\text{div}\,[\rho V\phi - \Gamma_\phi \text{grad}\phi] = S_\phi \tag{4}$$

where the first and second left-hand side terms are convection and diffusion, respectively; ϕ stands for the transported variable; Γ_ϕ is the appropriate diffusivity, and S_ϕ are as follows:

Mass source:

$$S_{\text{mass}} = \rho_g v_g \frac{A}{V}$$

The y-momentum source:

$$S_{\text{momentum}} = \rho_g v_g^2 \frac{A}{V}$$

Species (LiH) source:

$$S_{\text{LiH}} = \rho_g v_g \frac{A}{V}$$

Energy source:

$$S_{\text{energy}} = \rho_g v_g h_{950} \frac{A}{V} + \rho_g \frac{v_g^2}{2}$$

where A and V are, respectively, the area of the cell surface adjacent to the solid grain and the cell volume.

These sources are directly linked to Eqs. (2) and (3). Using Eq. (2) we define the gas mass flow rate as a function of the heat flux to the surface. Likewise, we calculate the local regression rate using Eq. (3). The all-important heat flux is calculated as a function of the solution for the gas-phase field (velocity, density, pressure, and temperature) above the surface.

To accomplish this task, we have used the standard wall function model to describe the thermal boundary layer in the user-defined functions (as for the momentum).

VI. Results

A. Cylindrical Configuration ($D_r = 1$)

Figure 5 shows the static temperature contours of both reacting and nonreacting cases. An intense flame is present over the fuel grain, growing along the combustor. Because of gas-phase combustion, the surface heat flux (Fig. 6) is up to 3 times that due only to convection from the hot airstream entering the combustor (in the nonreacting case).

The surface regresses at a rate comparable with that calculated by Jarymowycz et al. [12] (see Fig. 7). The total LiH mass flow rate injected into the chamber for the cylinder geometry is 0.065 kg/s and that of inlet air is 2.77 kg/s; thus, this scramjet combustor is working at an air-to-fuel ratio $A/F = 42.2$ (stoichiometric $A/F = 8.7$). Assuming Mach 7 flight conditions as in [12], the I_{sp} (defined as thrust-to-fuel mass flow rate ratio) is 11, 170 m/s and the specific thrust (thrust-to-air mass flow rate ratio) is 264 m/s; these values are slightly lower than those calculated in [5] at the same A/F

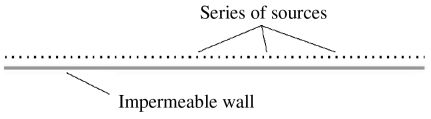

Fig. 4 Interface sources model.

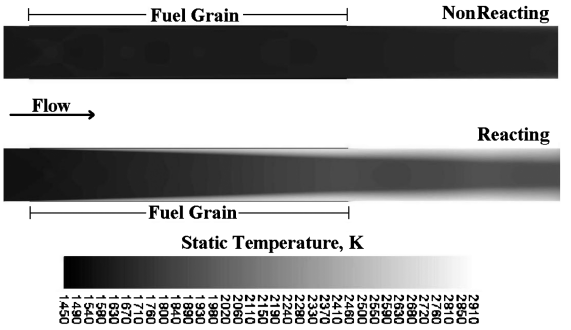

Fig. 5 Contours of static temperature (reacting and nonreacting case).

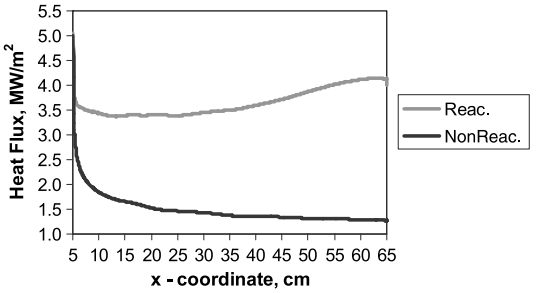

Fig. 6 Heat fluxes over the grain surface.

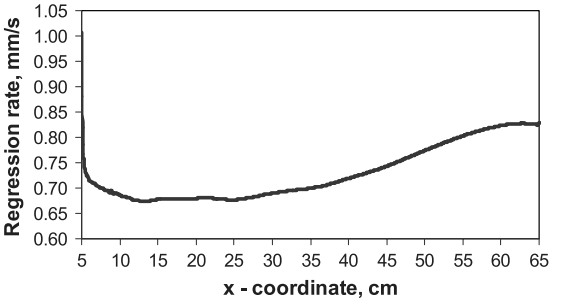

Fig. 7 Reacting grain: regression rate.

by means of an ideal SCRJ model. (The conventional I_{sp} and specific thrust in seconds can be obtained from these in SI units by simply dividing by $g = 09.81$ m/s^2.)

The temperature reached along the combustor peaks at 2950 K near the grain end (see Fig. 8). The sharp temperature increase for $x > 65$ (the final part of the grain) is connected to the end of the cooling effect due to the colder (950 K) LiH decomposition gases injected in the reacting boundary layer. Furthermore, at the end of the grain, where the mass injection ceases, the thickness of the reacting zone decreases slowly (Fig. 5), allowing expansion of the core flow. This effect is also visible in Fig. 9, in which the temperature along the half-radius line is compared with the nonreacting case (no blowing).

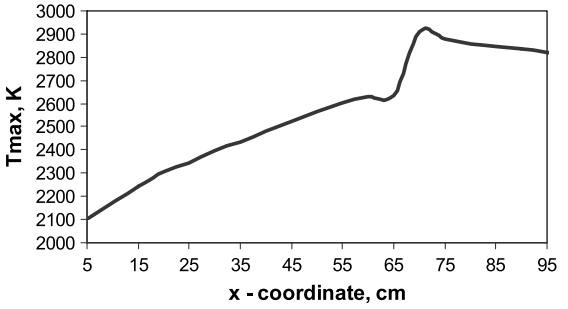

Fig. 8 Maximum static temperature at each x station.

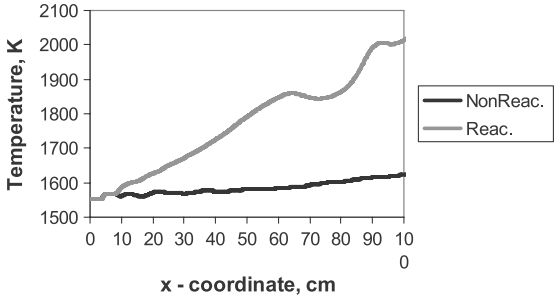

Fig. 9 Static temperature along the half-radius line.

Downstream of this first expansion, the reacting zone thickens due to increasing combustion temperature, driving a certain amount of flow recompression.

Figure 10 also shows the effect of the complex oblique shock system on the initial part of the grain (from $x = 0$ to 30 cm). An oblique shock is located exactly at the grain inlet; the compression, due to the shocks reflecting along the chamber, increases temperature and density and reduces blowing velocity. Note that despite the complex wave system, the flow at the exit section is still largely supersonic.

Figure 11 shows the contours of mixing time, calculated as

$$t = \frac{\eta^2}{D^{\text{th}}}$$

where D^{th} is the turbulent diffusivity and η is the Taylor scale, calculated as

$$\eta = \left(\frac{\nu k}{\varepsilon}\right)^{1/2}$$

where ν is the kinematic viscosity, k is the turbulent kinetic energy, and ε is the turbulent dissipation rate.

Because of the highly turbulent flow in the boundary layer, the mixing time is very short (on the order of 10^{-7} s); moreover, due to the growth of the boundary layer and to the consequent complex wave system, the mixing time decreases in the reacting core flow.

B. Dump Combustor (Configuration Dump05, $D_r = 1.1$)

Figure 12 shows the static temperature contours of both nonreacting and reacting cases. As we can see, an intense flame is also present over the fuel grain in this case, growing from the recirculation zone near the sudden area increase up to the exit section. Because of gas-phase combustion, the heat flux is 2–3 times higher than that due only to the hot flow entering the combustor in the nonreacting case.

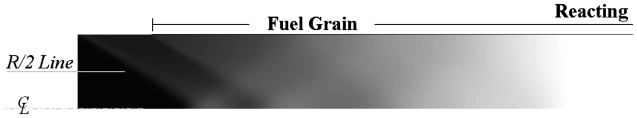

Fig. 10 Detail of the combustor (half-section) pressure field.

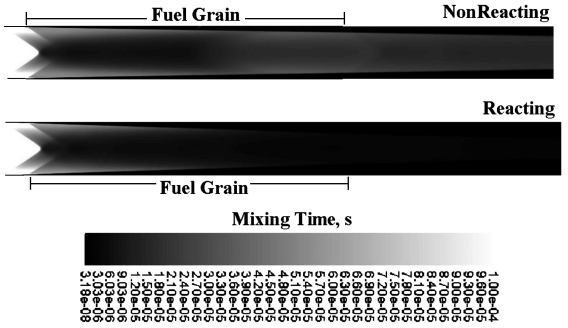

Fig. 11 Contour of mixing time (reacting and nonreacting case).

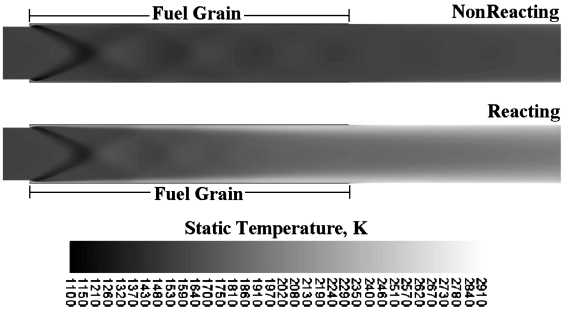

Fig. 12 Contours of static temperature (reacting and nonreacting case).

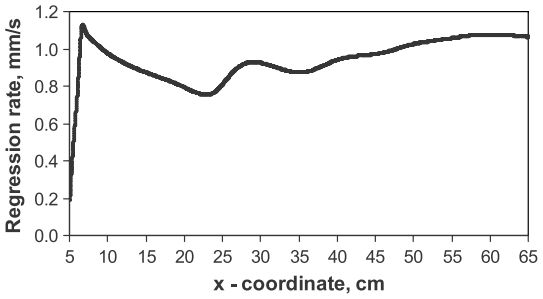

Fig. 13 Local regression rate.

The grain surface decomposes and regresses at roughly the same rate as that calculated by Ben-Arosh et al. [13] (see Fig. 13).

The LiH and air mass flow rates entering the combustor are 0.075 and 2.77 kg/s, respectively, ($A/F = 37.05$). Assuming conditions in [12], the SFSCRJ I_{sp} is 9620 m/s and the specific thrust is 260 m/s; these values are again slightly lower than in [5] with the ideal SCRJ model. The maximum temperature reached at each x station is plotted in Fig. 14; the peak is 2906 K.

Here, too, the temperature increases after the $x = 65$ cm station due to the end of the cooling effect of the gas injected from the grain surface. Furthermore, from $x = 10$ to 20 cm, there is cooling due to the expansion wave located near the upper corner of the dump. This effect is clearer when examining Fig. 15, which compares temperatures along the half-radius line in the reacting and nonreacting cases.

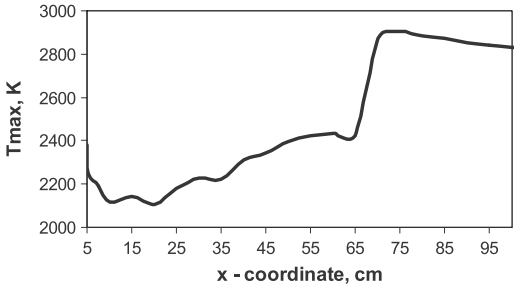

Fig. 14 Maximum static temperature at each x station.

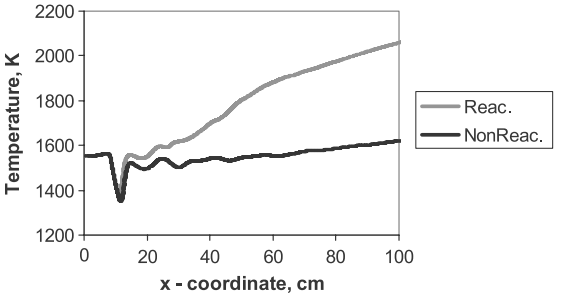

Fig. 15 Static temperature along the half-radius line.

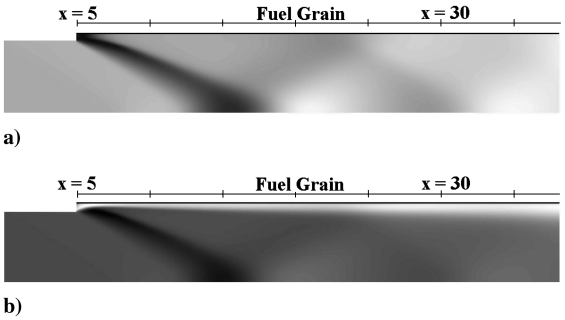

Fig. 16 Detail of reacting case: pressure (a) and temperature (b) fields.

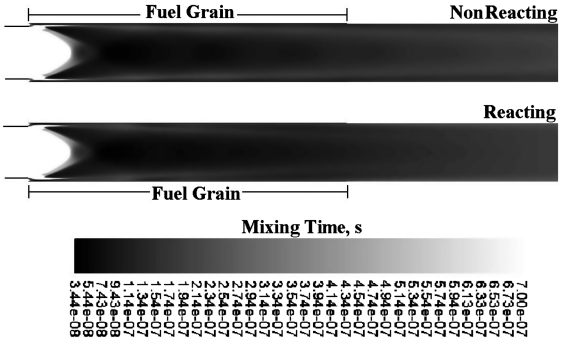

Fig. 17 Contour of mixing time (reacting and nonreacting case).

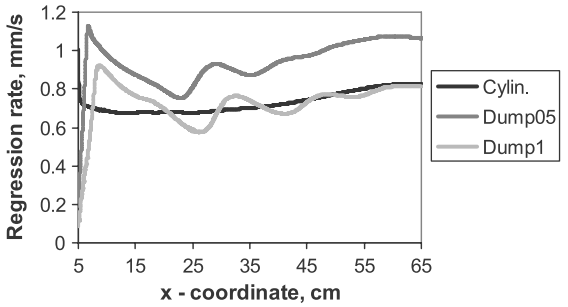

Fig. 18 Comparison among regression rates.

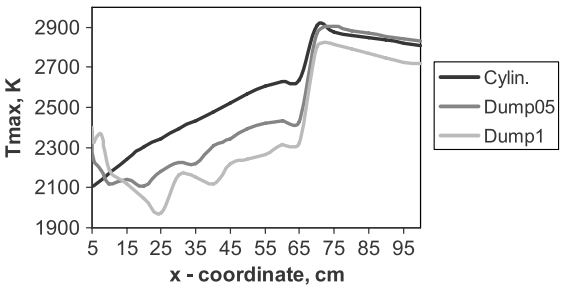

Fig. 19 Comparison among maximum static temperatures at each x station.

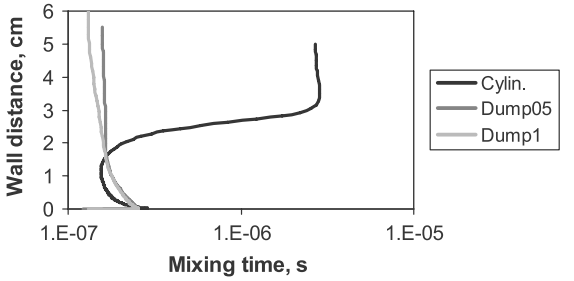

Fig. 20 Mixing times vs radius at $x = 85$ cm.

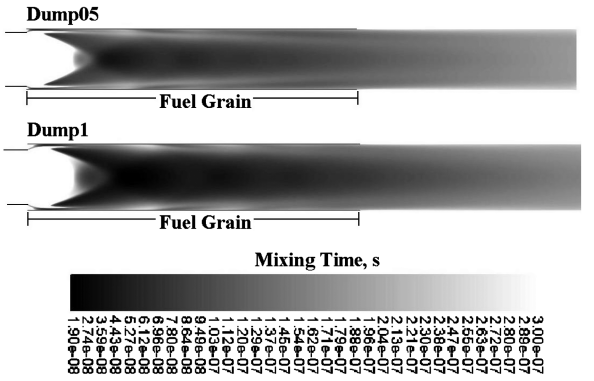

Fig. 21 Mixing time contours (dump05 vs dump1).

By comparing Figs. 12 and 15, it is clear that this expansion wave lowers the core flow temperature to 1300 K; the reflecting waves create alternatively compression and expansion regions, affecting greatly the reacting zone. Clearer details (from $x = 0$ to 30 cm) are in Fig. 16.

Figure 17 shows the mixing-time contours of nonreacting and reacting cases. Because of the short mixing times and the presence of a recirculation zone at the entrance, combustion temperatures are higher than in the cylindrical configuration and maintain a supersonic flow in the combustor exit section.

C. Configuration Dump1 ($D_r = 1.2$) and comparisons.

As in the case of $D_r = 1$ and 1.1, a flame develops along the combustor. The heat transfer is comparable with that for the cylindrical geometry, but at least 1 MW/m^2 lower than in dump05. As a consequence, regression rate (Fig. 18) and the maximum temperature at each x station (Fig. 19) are also lower than those of dump05.

This effect may be explained as follows: the larger step height (1 cm) allows more intense expansion and a larger chamber volume, lowering air temperatures more than the dump05 configuration. Thus, despite the improvement in mixing from $D_r = 1.1$ to 1.2 (Figs. 20 and 21), temperatures are lower. This behavior is confirmed by comparing the engine ideal performance, summarized in Table 5.

The effect of the increased dump height on combustion in the recirculation region near the inlet is shown in Figs. 22 and 23. A shorter dump height shortens mixing times in the corner, favoring flame holding and higher LiH decomposition rates injected in the reacting layer. That enhances combustion downstream of the boundary-layer—expansion-wave interaction zone.

The combined effect of enhanced mixing and decreased airflow temperature on H_2/O_2 and Li/O_2 rates is in Figs. 24 and 25. In dump05 and dump1 combustors, the H_2/O_2 reaction develops mainly over the grain, being more intense in the dump05 configuration and, consistently, more extended downstream for that of dump1. A similar trend holds for the Li/O_2 reaction, active mainly downstream, which penetrates the core flow before the exit section (see Fig. 25).

Table 5 Performance comparison

D_r	Specific thrust, m/s,	I_{sp}, m/s
1	264	11,170
1.1	260	9630
1.2	245	8160

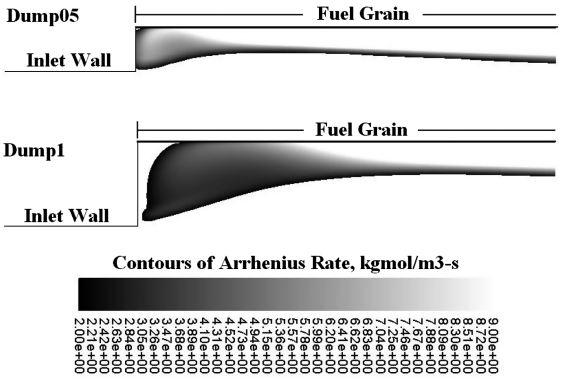

Fig. 22 Comparison among contours of H_2/O_2 reaction rate (dump05 vs dump1 details).

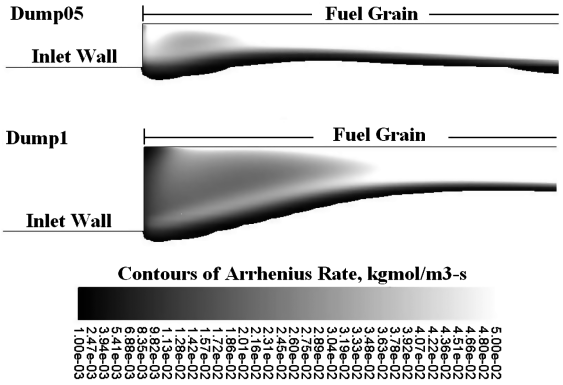

Fig. 23 Comparison among contours of Li/O_2 reaction rate (dump05 vs dump1 details).

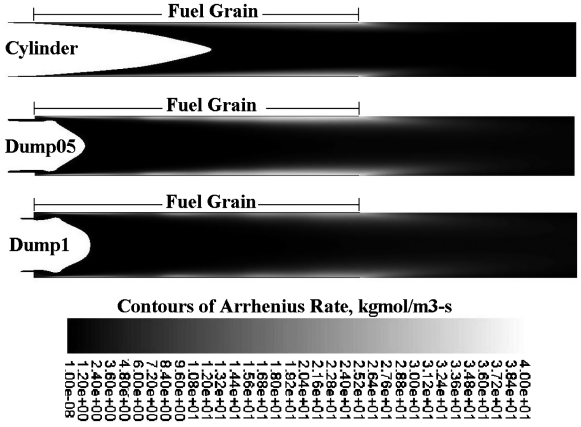

Fig. 24 Comparison among contours of H_2/O_2 reaction rate.

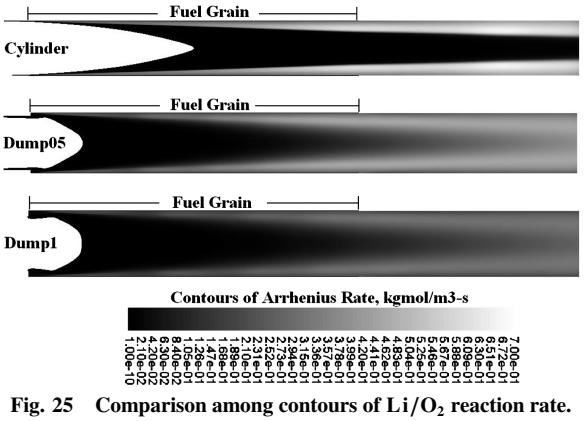

Fig. 25 Comparison among contours of Li/O_2 reaction rate.

VII. Conclusions

Supersonic combustion between solid LiH and air has been investigated with the goal of predicting the performance of LiH at conditions similar to those expected in a solid-fueled scramjet. A preliminary thermochemical analysis has identified the main species and reactions involved in the process: in particular, the presence of large amounts of hydrogen and Li produced by the thermal decomposition of LiH. Result suggest that at sufficiently high temperature, the species energetically most important, in addition to hydrogen, is liquid Li when reacting with air.

To overcome the lack of data concerning Li/air combustion, a parametric analysis has been carried out to predict chemical equilibria. Results show that at temperatures higher than 1100 K, Li does not react with air nitrogen; it produces mainly gaseous Li_2O, showing many similarities, in terms of equilibrium composition, with H_2/O_2 oxidation. A second thermochemical analysis has compared the reactions potentially involved in Li combustion, concluding that as a first approximation, the reaction scheme can be simplified, assuming one-step global reactions. Furthermore, these reaction rates may be plausibly described as proposed by Plane and Rajasekhar [41] for the reaction forming Li superoxide.

The physical model describing fuel blowing and decomposing from the grain surface has been developed by means of an order-of-magnitude analysis, showing that almost all liquid-Li droplets produced by decomposing LiH (and dragged away by the turbulent stream), vaporize and burn before exiting the combustor, contributing in a significant manner to heating and performance. The model for fuel blowing in the airstream from the decomposing LiH grain was implemented in the computational fluid dynamics code as a nonlinear boundary condition at the interface between the liquid surface and the reacting gas. Numerically, that translates to formulating mass, momentum, energy, and species sources located near the surface. This model predicts LiH regression rates that are comparable with those obtained by Jarymowycz et al. [12] and Ben-Arosh et al. [13].

Despite the limitations due to the standard $k-\varepsilon$ model and due to the assumption made about the Li/O_2 reaction rate, results are still intriguing. An intense flame zone is predicted to be present over the decomposing surface and downstream of the grain in the cylindrical configuration; the flame does not extinguish and high temperatures (on the order of 2900 K) are obtainable. Introducing a sudden cross-sectional enlargement (a dump) downstream of the inlet section, mixing in the combustor is enhanced, increasing the heat released to the core flow. Ideal specific impulse and thrust density predicted at a flight Mach $= 7$ are also interesting, being $10,000$ m/s and 200–300 m/s, respectively. However, an excessive dump ratio decreases the core flow temperature (due to expansion waves) and increases the combustor volume, lowering combustor performance.

To conclude from this preliminary investigation, LiH seems a good candidate for solid-fueled scramjet applications, behaving as an high-energy-density bifuel system but also as a safe and compact hydrogen carrier.

References

[1] Simone, D., and Bruno, C., "LiH for Microrockets Applications," *2nd International Conference on Green Propellants* [CD-ROM], ESA Publ. Div., Noordwijk, The Netherlands, 2004.

[2] Chiaverini, M. J., and Kuo, K. K., "Fundamentals of Hybrid Rocket Combustion and Propulsion," *Progress in Astronautics and Aeronautics*, Vol. 128, AIAA, Reston, VA, 2007, pp. 421–423.

[3] Simone, D., and Bruno, C., "LiH as Fuel for Aerospace Propulsion," *25th ISTS* [CD-ROM], Japan Society for Aeronautical and Space Sciences, Tokyo, June 2007, Paper 2006-a-38.

[4] Ju, Y., and Austin, J., "AIAA—The Year in Review," *Aerospace America*, Vol. 44, Dec. 2006, p. 55.

[5] Simone, D., "Analysis of LiH Combustion in Solid-Fueled Scramjet Engine," Ph.D. Dissertation, Dept. of Mechanics and Aeronautics, Univ. of Rome "La Sapienza," Rome, Feb. 2008.

[6] Clifton, D. G., and Sitney, L. R., "Theoretical Specific Impulses of Lithium-Based Propellant Systems in Nuclear and Chemical Rockets," Los Alamos Scientific Lab., Rept. LA-2276 Los Alamos, NM, 1959.

[7] Pourpoint, T. L., and Rusek, J. J., "Novel Organometallic Propellants for Hypergolic Applications," *5th International Hydrogen Peroxide Propulsion Conference*, Purdue Univ., West Lafayette, IN, Sept. 2002, pp. 163–170.
[8] Gordon, S., and McBride, J. B., "Computer Program for Calculation of Complex Chemical Equilibrium Compositions and Applications," NASA Lewis Research Center, Ref. Publ. 1311, Cleveland, OH, Oct. 1994.
[9] Ben-Arosh, R., Natan, B., Spiegler, E., and Gany, A., "Theoretical Study of a Solid Fuel Scramjet Combustor," *Acta Astronautica*, Vol. 45, No. 3, 1999, pp. 155–166. doi:10.1016/S0094-5765(99)00113-7
[10] Ben-Yakar, A., Natan, B., and Gany, A., "Investigation of a Solid Scramjet Combustor," *Journal of Propulsion and Power*, Vol. 14, No. 4, 1998, pp. 447–455. doi:10.2514/2.5321
[11] Cohen-Zur, A., and Natan, B., "Experimental Investigation of a Supersonic Combustion Solid Fuel Ramjet," *Journal of Propulsion and Power*, Vol. 14, No. 6, 1998, pp. 880–889. doi:10.2514/2.5379
[12] Jarymovycz, T. A., Yang, V., and Kuo, K. K., "Numerical Study of Solid-Fuel Combustion Under Supersonic Crossflows," *Journal of Propulsion and Power*, Vol. 8, No. 2, 1992, pp. 346–353. doi:10.2514/3.23484
[13] Ben-Arosh, R., Natan, B., Spiegler, E., and Gany, A., "Fuel–Air Mixing in Solid Fuel Scramjet Combustor," *International Journal of Turbo and Jet Engines*, Vol. 15, No. 3, 1998, pp. 223–234.
[14] Welch, F. H., "LiH Properties," General Electric Co., Aircraft Nuclear Propulsion Dept., Rept. DC 61-3-73, Cincinnati, OH, Mar. 1961.
[15] Holley, C. E., Jr., Challenger, G. E., and Pavone, D., "The Preparation of Pure LiH," Los Alamos Scientific Lab., Rept. LA-1705 Los Alamos, NM, 1955.
[16] Brinza, V. N., Bavaitsev, I. V., and Papaev, S. T., "Investigation of the Combustion Rate of Aerosuspensions of LiH Powder," *Combustion, Explosion, and Shock Waves*, Vol. 15, No. 1, 1979, pp. 100–101. doi:10.1007/BF00785341
[17] Odgers, J., and Kretschmer, D., *Gas Turbine Fuels and their Influence on Combustion*, Abacus, Kent, England, U.K., 1986, pp. 14–15.
[18] Veleckis, E., Van Deventer, E. H., and Blander, M., "The Li–LiH System," *Journal of Physical Chemistry*, Vol. 78, No. 19, 1974, pp. 1933–1940. doi:10.1021/j100612a013
[19] Vogt, J. V., "Measurement of Thermal Properties of LiH and LiH-Li Mixtures: Enthalpy, Heat of Fusion, Conductivity," TAPCO—Thompson Ramo Wooldridge, Inc., Rept. ER-4809, Cleveland, OH, 1962.
[20] Shpil'rayn, E. E., Yakimovich, K. A., Kagan, D. N., and Shval'b, V. G., "A Theoretical and Experimental Study of the Thermophysical Properties of LiH," NASA TT-20179, Apr. 1988.
[21] Yakimovich, K. A., Tsitsarkin, A. F., and Mozgovoi, A. G., "Experimental Investigation of the Density of Liquid LiH at High Temperatures," *High Temperature*, Vol. 38, No. 6, 2000, pp. 867–874. doi:10.1023/A:1004133121642
[22] Kawano, H., Zhu, Y., and Tanaka, A., "Thermal desorption of H2, H- and Electron by Temperature-Programmed Heating of Saline Hydrides in Vacuum," *Thermochimica Acta*, Vol. 344, Nos. 1–2, 2000, pp. 119–125. doi:10.1016/S0040-6031(99)00334-2
[23] Mayer, S. W., and Schieler, L., "Computed Activation Energies and Rate Constants for Forward and Reverse Transfers of Hydrogen Atoms," *Journal of Physical Chemistry*, Vol. 72, No. 1, 1968, pp. 236–240. doi:10.1021/j100847a044
[24] Mayer, S. W., Schieler, L., and Johnston, H., "Computed High-Temperature Rate Constant for Hydrogen-Atom Transfers Involving Light Atoms," *Journal of Chemical Physics*, Vol. 45, No. 1, July 1966, pp. 385–391. doi:10.1063/1.1727340
[25] Jerry, B., and Modisette, L., "Preliminary Investigation of LiH as High-Temperature Internal Coolant," NACA RM L57B12a, 1957.
[26] Jerry, B., and Modisette, L., "Investigation of LiH and Magnesium as High-Temperature Internal Coolants with Several Skin Materials," NACA RM L58B17, 1958.
[27] Jeppson, D. W., "Interaction of Liquid Li with Various Atmospheres, Concretes, and Insulating Metals; and Filtration of Li Aerosols," Hanford Engineering Development Lab., Rept. HEDL-TME 79-7, Hanford, WA, 1978.
[28] Davison, H. W., "Compilation of Thermophysical Properties of Liquid Lithium," NASA TN D-4650, July 1968.
[29] Jaynes, G. E., and Hanks, G. S., Taub, J. M., and Doll, D. T., "The Fabrication of Lithium," Los Alamos Scientific Lab., Rept. LA-1191, Los Alamos, NM, Jan. 1951.
[30] Williams, R. K., Coleman, G. L., and Yarbrough, D. W., "An Evaluation of Some Thermodynamic and Transport Properties of Solid and Liquid Li over the Temperature Range 200–1700 K," Oak Ridge National Lab., Rept. ORNL/TM-10622, Oak Ridge, TN, Mar. 1988.
[31] Dube, D. A., and Kazimi, M. S., "Analysis of Design Strategies for Mitigating the Consequences of Li Fire Within Containment of Controlled Thermonuclear Reactors," Dept. of Nuclear Engineering, Massachusetts Inst. of Technology, Rept. MITNE-219, Cambridge, MA, July 1978.
[32] Bohachevsky, I. O., Booth, L. A., and Hafer, J. F., "Li Flow on the Inside of a Spherical Fusion-Reactor Cavity," Los Alamos Scientific Lab.,, Rept. LA-6362-MS, Los Alamos, NM, June 1976.
[33] Tillack, M., and Kazimi, M. S., "Development and Verification of the LITFIRE Code for Predicting the Effects of Li Spills in Fusion Reactor Containments," Dept. of Nuclear Engineering, Massachusetts Inst. of Technology, Rept. PFC/RR-80-11, Cambridge, MA, July 1980.
[34] Gilberti, V. J., and Kazimi, M. S., "Modeling of Li and Lithium-Lead Reactions in Air Using LITFIRE," Plasma Fusion Center, Dept. of Nuclear Engineering, Massachusetts Inst. of Technology, Rept. PFC/RR-83-08, Cambridge, MA, Jan. 1983.
[35] Gil, T. K., and Kazimi, M. S., "The Kinetics of Li Reaction with Oxygen-Nitrogen Mixtures," Plasma Fusion Center, Dept. of Nuclear Engineering, Massachusetts Inst. of Technology, Rept. PFC/RR-86-1, Cambridge, MA, Jan. 1986.
[36] Barnett, D. S., and Kazimi, M. S., "Consequence of a Li Spill Inside the Containment and Vacuum Torus of a Fusion Reactor," Plasma Fusion Center, Dept. of Nuclear Engineering, Massachusetts Inst. of Technology, Rept. PFC/RR-87-9, Cambridge, MA, June 1987.
[37] Barnett, D. S., and Kazimi, M. S., "The Chemical Kinetics of the Reactions of Li with Steam-Air Mixtures," Plasma Fusion Center, Dept. of Nuclear Engineering, Massachusetts Inst. of Technology, Rept. PFC/RR-89-3, Cambridge, MA, Apr. 1989.
[38] Utschig, T. T., and Corradini, M. L., "Computer Modeling for Li Safety in Fusion Systems: LINT and MELCOR," Fusion Technology Inst., Univ. of Wisconsin, Rept. UWFDM-1101, Madison, WI, June 1999.
[39] Merrill, B. J., "Modification Made to the MELCOR Code for Analyzing Li Fires in Fusion Reactors," Idaho National Engineering and Environmental Lab., Rept. INEEL/EXT-2000-00489, Idaho Falls, ID, Apr. 2000.
[40] Patrick, R., and Golden, D. M., "Termolecular Reaction of Alkali Metal Atoms with O2 and OH," *International Journal of Chemical Kinetics*, Vol. 16, No. 12, 1984, pp. 1567–1574. doi:10.1002/kin.550161210
[41] Plane, J. M. C., and Rajasekhar, B., "A Study of the Reaction Li + O_2 + M (M = N_2, He) over the Temperature Range 267–1100 K by Time Resolved Laser-Induced Fluorescence of Li ($2^2P_J - 2^2S_{1/2}$)," *Journal of Physical Chemistry*, Vol. 92, No. 13, 1988, pp. 3884–3890. doi:10.1021/j100324a041
[42] Anon., "NIST Chemistry WebBook," *NIST Standard Reference Database No. 69* [online database], http://webbook.nist.gov/chemistry/ [retrieved May 2008].
[43] Sutton, G. P., *Rocket Propulsion Elements: An Introduction to the Engineering of Rockets*, Wiley, New York, 1992.
[44] Carmicino, C., "Alcuni Aspetti della Balistica Interna di un Endoreattore a Propellenti Ibridi e del Comportamento di Ugelli a Spina Troncata," Ph.D. Dissertation, Dept. of Space Science and Engineering, Univ. of Naples "Federico II," Naples, Italy, 2002.
[45] Schlichting, H., *Boundary-Layer Theory*, McGraw–Hill, New York, 1979, pp. 645–647.
[46] FLUENT, Software Package, Ver. 6.2.16, ANSYS, Inc., Canonsburg, PA, 2007.
[47] Fournier, C., Michard, M., and Bataille, F., "Numerical Simulations of a Confined Channel Flow Driven by Non-Isothermal Wall Injection," *Progress in Computational Fluid Dynamics*, Vol. 6, Nos. 1–3, 2006, pp. 129–136. doi:10.1504/PCFD.2006.009490

C. Segal
Associate Editor